Structure, Vol. 11, 591–603, May, 2003, ©2003 Elsevier Science Ltd. All rights reserved. DOI 10.1016/S0969-2126(03)00074-1

tRNA-Dependent Active Site Assembly in a Class I Aminoacyl-tRNA Synthetase

Luke D. Sherlin and John J. Perona*
Department of Chemistry and Biochemistry and
Interdepartmental Program in Biomolecular
Science and Engineering
University of California, Santa Barbara
Santa Barbara, California 93106

Summary

The crystal structure of ligand-free *E. coli* glutaminyl-tRNA synthetase (GlnRS) at 2.4 Å resolution shows that substrate binding is essential to construction of a catalytically proficient active site. tRNA binding generates structural changes throughout the enzyme, repositioning key active site peptides that bind glutamine and ATP. The structure gives insight into long-standing questions regarding the tRNA dependence of glutaminyl adenylate formation, the coupling of amino acid and tRNA selectivities, and the roles of specific pathways for transmission of tRNA binding signals to the active site. Comparative analysis of the unliganded and tRNA-bound structures shows, in detail, how flexibility is built into the enzyme architecture and suggests that the induced-fit transitions are a key underlying determinant of both amino acid and tRNA specificity.

Introduction

Aminoacyl-tRNA synthetases (aaRSs) catalyze the specific linkage of an amino acid to cognate tRNAs in a two-step reaction that proceeds via an activated aminoacyl-adenylate intermediate [1]. The enzymes are grouped into two classes on the basis of distinctive active site folds possessing mutually exclusive primary sequence motifs [2]. Extensive phylogenetic and structural analyses form the basis for further subclassifications, which may reflect evolutionary origins [3, 4]. All class I enzymes possess a common parallel β sheet Rossman dinucleotide fold at their N termini, which binds ATP, amino acid, and the 3′-terminus of tRNA [5, 6]. The fold contains a common domain insertion between the two pseudosymmetrical halves, which orients the acceptor end of the tRNA into the active site and is expanded to contain a hydrolytic editing site in ValRS, IleRS, and LeuRS [7–10]. The C-terminal domains provide additional tRNA specificity, including interactions with the anticodon nucleotides. A centrally located helical subdomain links the second half of the dinucleotide fold with the anticodon binding region and helps to globally orient the tRNA on the surface of the enzyme [11].

It has become increasingly apparent that aaRSs achieve their remarkable specificities for amino acid and tRNA, in part, through induced-fit conformational changes. Both biochemical studies and comparisons of X-ray structures in different liganded states provide compelling evidence of this phenomenon. For example, amino acid binding leads to structural changes of varying degree in CysRS, MetRS, ArgRS, and TyrRS [12–15]. Similarly, formation of the aminoacyl adenylate in TyrRS, TrpRS, and LeuRS also causes conformational rearrangements, including positioning of the catalytically essential lysine within the conserved KMSKS sequence motif [10, 15, 16]. Finally, comparisons of tRNA-bound and unbound structures of GluRS, ArgRS, TyrRS, and IleRS reveal induced structural reorganization, including side chain movements, loop ordering, and domain rotations [7, 14, 15, 17]. Interestingly, despite the conserved Rossman fold, the conformational changes upon ligand binding are not conserved but, instead, appear idiosyncratic among the class I enzymes. For example, the degree of reorganization in response to tRNA binding varies widely, from global movement of the editing domain in IleRS [7] to small local differences in TyrRS [15].

The central and ancient function of tRNA synthetases in translation, their potential for impact in biotechnology and medicine through drug design and protein engineering approaches, and their newly appreciated roles in other physiological processes highlight the importance of thoroughly understanding the aminoacylation mechanism for all enzymes in the family [18]. Here we focus on *E. coli* glutaminyl-tRNA synthetase (GlnRS), a canonical monomeric class I enzyme with a molecular weight of 63 kDa. X-ray structures of GlnRS are available bound in ternary complexes with $tRNA^{Gln}$ and either ATP, AMP, or a glutaminyl-adenylate analog [6, 19–21] (Figure 1). Considerable biochemical and genetic evidence suggests that induced-fit conformational changes play an important role in the GlnRS mechanism (reviewed in [22]). For example, both fluorescence and neutron solution scattering experiments have yielded direct physical evidence for enzyme rearrangements upon tRNA binding [23–25]. Mutation of $tRNA^{Gln}$ anticodon nucleotides sharply reduces the k_{cat} for aminoacylation and also influences the K_m for glutamine [26, 27], suggesting the existence of structural pathways for communication from the C-terminal β barrrel domains to the active site some 40 Å distant. The kinetic study of $tRNA^{Gln}$ species mutated in the D and variable loops also suggests a pathway for communication from the globular hinge region to the active site [28, 29]. Finally, GlnRS is one of four class I tRNA synthetases that require tRNA binding for adenylate synthesis, suggesting that the large substrate may be required to fully form the active site structure [30].

A variety of experiments have implicated specific peptide segments and amino acids in GlnRS as important to aminoacylation efficiency and specificity in vivo and in vitro [31–33]. One proposal suggests that a long loop inserted into one anticodon binding β barrel mediates communication by packing onto sequences adjacent to the KMSKS catalytic motif ([6]; Figure 1). An alternative

*Correspondence: perona@chem.ucsb.edu

Key words: induced fit; substrate specificity; RNA-protein interactions; translation

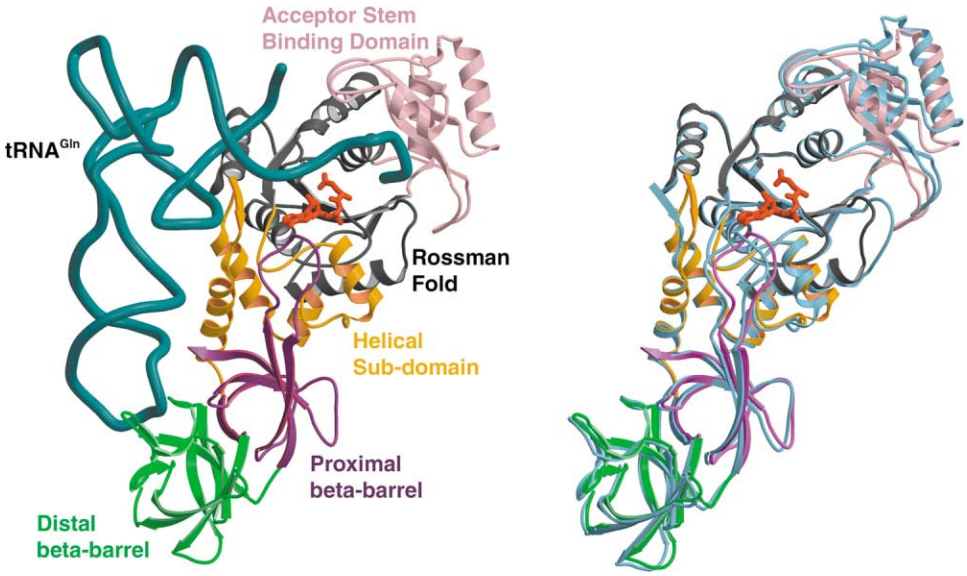

Figure 1. Structures of Unliganded and tRNA-Bound GLNRS

(A) Ribbon model of the GlnRS backbone as visualized in the ternary complex bound to $tRNA^{Gln}$ and QSI (5′-O-[N-(L-glutaminyl)sulphamoyl] adenosine; [21]). Domains are colored as follows: dinucleotide Rossman fold (DNF), gray; acceptor stem binding domain (ABD), pink; helical subdomain, orange; proximal β barrel, magenta; distal β barrel, green. tRNA backbone, blue; QSI aminoacyl adenylate analog, red.

(B) Superposition of the GlnRS-$tRNA^{Gln}$-QSI ternary complex with unliganded GlnRS. Ribbon model of the unliganded enzyme, light blue; complexed enzyme, colored as in (A). The structures were aligned by backbone atoms in the dinucleotide binding fold (see text for details).

hypothesis is that anticodon or hinge region recognition is connected to the active site via a long helix in the helical subdomain, which runs from the tRNA inner elbow to the anticodon stem [29, 31, 32]. To evaluate these proposals, we have determined the crystal structure of unliganded *E. coli* GlnRS at 2.4 Å resolution. Comparison of this structure with the tRNA-bound complexes reveals that tRNA binding generates subtle, but significant, conformational changes in several regions of the protein, particularly in, and adjacent to, the active site cleft. These data provide a structural basis for exploring the induced-fit component of tRNA and amino acid specificity.

Results

High-resolution structures of the *E. coli* GlnRS-$tRNA^{Gln}$ complex have previously been determined in an orthorhombic crystal lattice in which the enzyme retains catalytic activity [6, 19–21]. In these structures the α-phosphate of ATP, the 3′-terminal A76 ribose of tRNA, and the α-carboxylate of glutamine are closely juxtaposed, allowing construction of a detailed stereochemical model for the transition state of glutaminyl adenylate formation [20, 34]. However, no significant structural differences in the enzyme are observed among any of the complexes bound to ATP, AMP, glutamine, or the adenylate analog 5′-O-[N-(L-glutaminyl)sulfamoyl]adenosine (QSI). Thus, the conformational pathway for approach to the transition state, implicated by numerous biochemical experiments, has remained unresolved. The structure of the unliganded enzyme in a new crystalline environment now reveals the ligand-dependent induced-fit transitions in atomic detail.

Overall Structural Characteristics

The structure of unliganded GlnRS was determined by molecular replacement methods with the tRNA cocrystal as search model and was refined to 2.4 Å resolution with tight stereochemical constraints (see Table 1 and Experimental Procedures). A total of 521 of the 553 amino acids could be built into the electron density maps. The only fully disordered regions comprise (1) the amino-terminal pentapeptide, the carboxy-terminal heptapeptide, and a 13-amino acid surface loop in one of the anticodon binding C-terminal β barrels, almost all of which (22 of the 25 residues) were also disordered in the tRNA-bound complex; (2) three amino acids in a surface loop containing a short β strand, which binds at the extreme inside corner of the tRNA L shape (amino acids 315–322); (3) one amino acid in a surface loop comprising amino acids 64–76 of the dinucleotide fold (DNF), which adopts a new conformation in the unliganded enzyme; and (4) two amino acids in separate surface loops in the C-terminal β barrel domains, which are less well-ordered in the unliganded enzyme.

The overall Wilson B factors and numerically averaged atomic B factors for unliganded GlnRS are approximately 60 $Å^2$, significantly higher than those for the tRNA cocrystal structures (Table 1). To better assess the extent of atomic mobility and to reduce ambiguity with respect to interpreting conformational rearrangements, we refined the structure independently from two different data sets at resolutions of 2.4 Å and 2.65 Å, respectively (Table 1; data sets 1 and 2). Superposition of polypeptide backbone atoms (N, Cα, C, and O) revealed an rms difference of 0.98 Å over the entire structures. This is somewhat higher than anticipated on the basis of expected positional errors at this resolution, reflecting

Table 1. X-Ray Data Collection and Refinement Statistics

	Data Set 1	Data Set 2	Data Set 3
Radiation source	SSRL BL 11-1	SSRL BL 7-1	RAXIS II (Cu)
Growth conditions	10% PEG 1000 10% PEG 8000 0.1 M sodium acetate 5 mM AMPCPP 0.1 M PIPES (pH 7.5)	PEG 2000 MME 0.1 M sodium acetate 0.1 M PIPES (pH 7.5) 5 mM AMPCPP	PEG 2000 MME 0.1 M sodium acetate 0.1 M PIPES (pH 7.5) 5 mM AMPCPP
Cell constants	$P2_12_12_1$	$P2_12_12_1$	$P2_12_12_1$
a, b, c (Å)	41.40, 64.12, 208.9	41.39, 64.16, 207.7	41.33, 64.25, 207.7
α, β, γ (°)	90.0, 90.0, 90.0	90.0, 90.0, 90.0	90.0, 90.0, 90.0
Resolution range	30.0–2.40	30.0–2.65	30.0–2.80
Reflections (unique)	141,412 (21,185)	177,476 (15,296)	162,627 (11,578)
R_{merge}	5.9 (37.8)	10.4 (33.5)	11.3 (43.7)
I/σ	14.1 (2.8)	11.2 (3.4)	7.9 (1.8)
Completeness (%)	93.5 (95.8)	90.3 (76.3)	79.4 (82.4)
Multiplicity	3.7 (3.6)	4.0 (3.8)	2.2 (2.1)
Wilson B factor (Å^2)	64.1	62.8	57.7
R_{cryst} (R_{free})	24.5% (33.4%)	24.6% (31.0%)	
Rmsd bonds (Å)	0.007	0.011	
Rmsd angles (°)	1.23	2.03	

the relatively high mobilities. However, the extent of local variability correlates well with the thermal factors (Figure 2A), suggesting that the latter indeed reflect atomic motions. The greatest deviations are in the anticodon binding C-terminal β barrels, consistent with the observation that these domains are also more mobile when bound to tRNA [6, 19]. The following description is based on the 2.4 Å resolution structure, and all depicted rearrangements are in segments retaining high structural similarity between the two unliganded models, with clear differences to the tRNA-bound state. Simulated-annealing electron density maps (Figure 2B) are of consistently higher quality for the 2.4 Å structure, despite the slightly higher R_{free} in this case (Table 1).

The two structures were determined from crystals grown in the presence of the ATP analog AMPCPP. However, no electron density corresponding to any part of this inhibitor was visible in electron density maps. Difference electron density maps calculated at 3.0 Å resolution, with data collected on crystals grown instead in the presence of 5 mM ATP, similarly failed to show evidence for ligand binding (data not shown). Interestingly, the inclusion of 2 mM glutamine in crystallization drops containing either ATP or AMPCPP inhibits crystal formation. Further, soaking preformed crystals in solutions containing 0.5 mM–10 mM glutamine resulted in severe deterioration of diffraction. These observations suggest that glutamine may bind GlnRS in the absence of tRNA, generating a conformational change that either prevents crystal growth under these conditions or results in disruption of preformed lattice contacts (see Discussion).

There are no global differences between the unliganded and tRNA-bound GlnRS structures. The largest reorganization upon tRNA binding occurs in the acceptor binding domain (ABD), which is inserted between the two halves of the dinucleotide fold (DNF) (Figures 1B and 3A). tRNA binding causes the ABD to make a rigid body rotation of 10° in the direction of the DNF, resulting in the reorganization of a DNF surface loop that contains amino acid binding determinants. The orientation of the two anticodon binding β barrel domains (ACB) with respect to the DNF is only subtly changed upon tRNA binding. However, a surface loop binding at the inner corner of the tRNA L shape (inner corner loop [ICL]) is less well ordered and adopts a different conformation in the unliganded enzyme. In turn, adjacent peptide segments in the centrally located helical subdomain, together with a long hairpin loop emanating from the proximal β barrel, are subtly reorganized. These movements impact the interface between the helical subdomain and the DNF and rearrange the position of active site groups to block productive ATP and glutamine binding in the absence of tRNA.

Induced-Fit Conformational Transitions

Interactions between the ABD and the DNF Domain

The dinucleotide folds of the unliganded and tRNA-bound enzyme were carefully superimposed to assess the extent of structural conservation in the catalytic domain. Backbone atoms of 94 amino acids comprising residues 25–31, 36–63, 77–99, 213–239, and 252–260 from the tRNA-bound structure could be superimposed on their counterparts in the unliganded enzyme with an rms deviation in position of 0.50 Å, indicating close similarity. This superposition reveals a 10° reorientation of the inserted ABD (amino acids 100–210) in the direction of the active site (Figure 3A). Further superpositions also showed that the α/β fold of the ABD is very well maintained during tRNA binding (rms deviation of 0.39 Å for superposition of backbone atoms in 94 amino acids comprising residues 101–134, 141–194, and 205–210; Figure 3B). However, two surface loops at positions 135–140 (bridging αE to β5; Figures 3 and 4) and 195–204 (bridging β7 to β8) in the ABD do show small rearrangements. The first of these contains the Leu136 side chain, which stacks between A72 of the disrupted U1-A72 base pair, and the intact G2-C71 pair in the tRNA-bound structure (Figure 3B, "Unpairing Loop"). Interestingly, while this loop is very well conserved among prokaryotic GlnRS structures, it is of variable length and sequence in eukaryotes (Figure 4). Further,

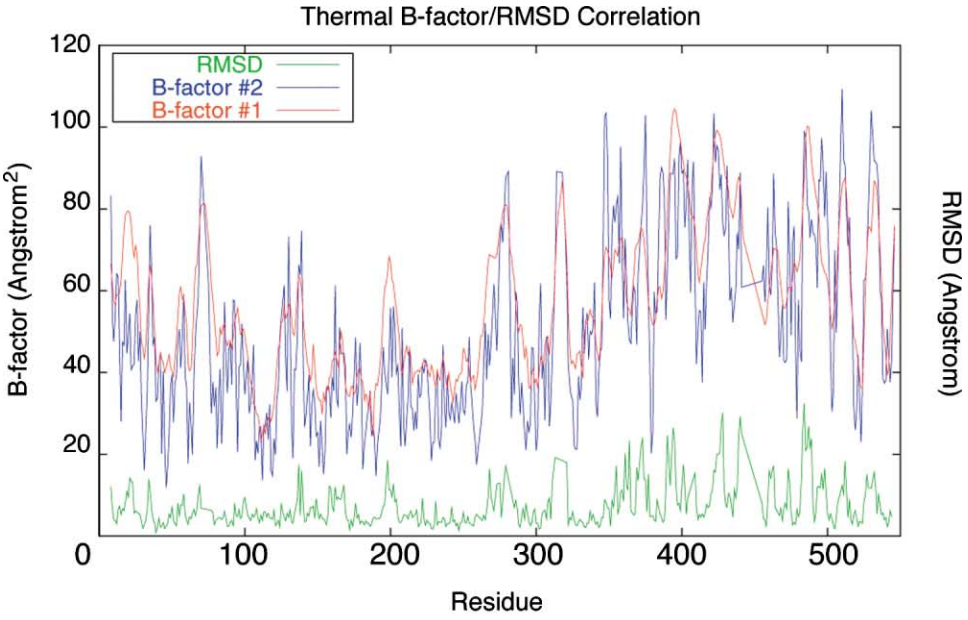

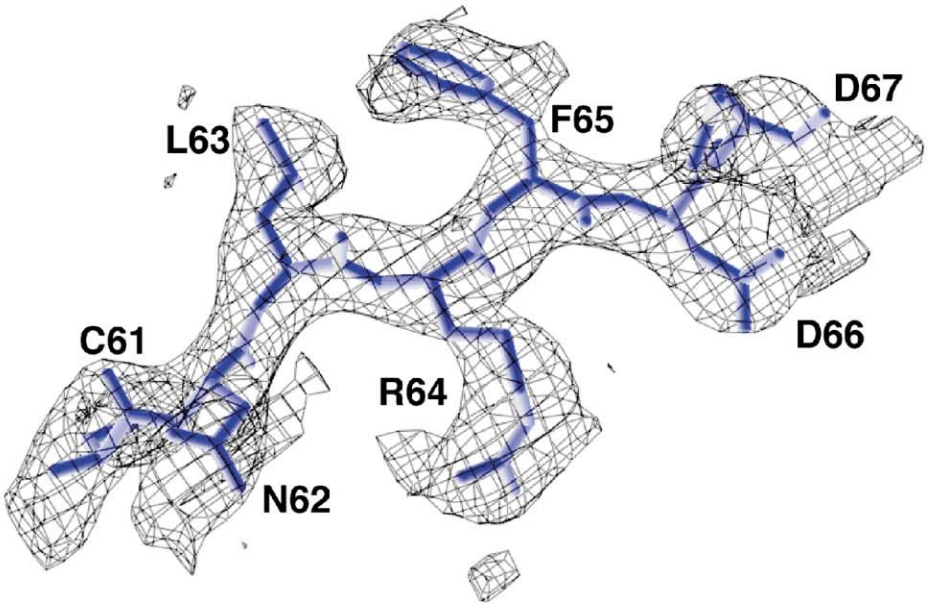

Figure 2. Validation of Unliganded Structure Models

(A) Analysis of thermal factors and rms deviations in the two unliganded structure models. The B factor (in Å^2) is on the left ordinate, and the rms deviation in position of backbone atoms in equivalent residues (in Å) is on the right ordinate (delineated in increments of 2Å). To determine the rms deviations, we superimposed the two unliganded models with all α carbon atoms in the protein structures.

(B) Simulated annealing OMIT electron density map at strand β2 in the DNF, for the higher-resolution structural model. The map is calculated in the range 6.0–2.4 Å and is displayed at the 1.0 σ level.

eukaryotic tRNA^{Gln} acceptors contain a strong G1-C72 terminal acceptor-stem pair instead of the more easily disrupted U1-A72 or A1-U72 pairs found in all bacterial tRNA^{Gln} acceptors. Thus, the mechanisms to facilitate tRNA^{Gln} 3′-end hairpinning may differ in the bacterial and eukaryotic domains.

The 10° rotation of the ABD creates a complementary interface for binding the hairpinned 3′-terminus of tRNA^{Gln}, including the formation of ionic and other interactions with the sugar-phosphate backbone and a well-developed pocket for the unstacked cytidine ring of C74 ([6]; Figure 5A). At the tRNA 3′-terminal dinucleotide, phosphate contacts are made by the side chains of Lys192 and Arg194, directly adjacent to the surface loop at positions 195–204, which is displaced in the unliganded enzyme. Significantly, in the tRNA complex, Arg194 is also involved in intramolecular contacts with Asn69 of the DNF, which also makes hydrogen bonds

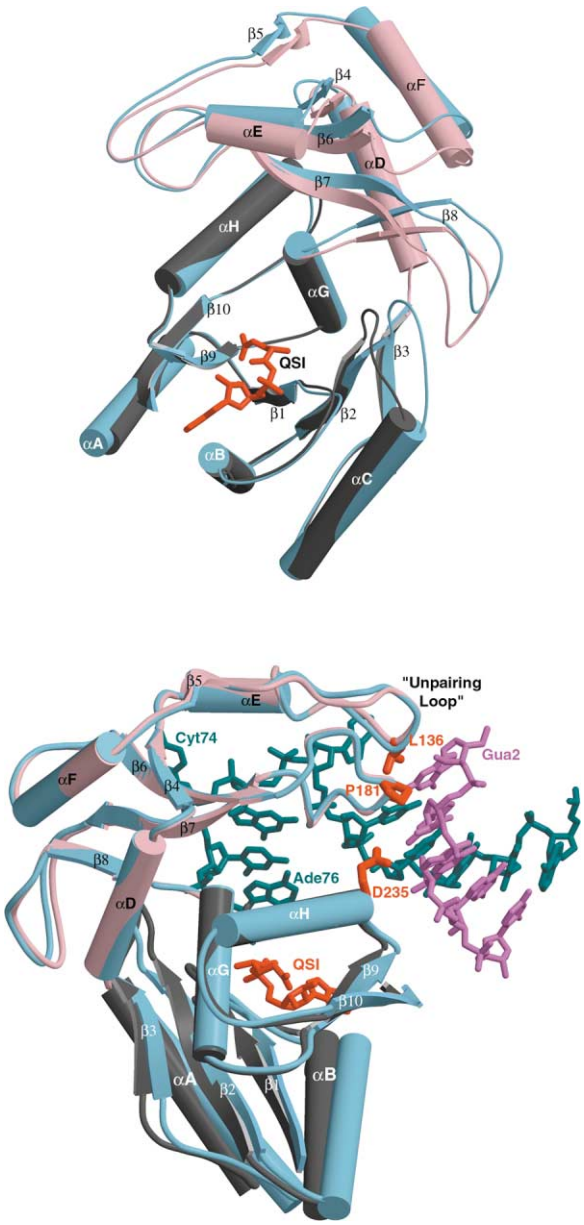

Figure 3. Domain Rearrangements in GlnRS

(A) Superposition of tRNA-complexed (gray and pink) and unliganded (blue) GlnRS by backbone atoms in the DNF domain (see text for details). The ABD (pink) rotates as a rigid body, with the largest movement in the loop spanning amino acids 194–205, bridging strands β7 and β8 (right). The reoriented loop in the DNF, which bridges β2 and αC and interacts with QSI (bottom right), is not included in the superimposed atoms.

(B) Superposition of tRNA-complexed (pink) and unliganded (blue) GlnRS by backbone atoms in the ABD (see text for details). The hairpinned tRNA acceptor stem is at the right. Amino acids Leu136, Pro181, and Asp235, emanating from three secondary structure elements binding in the minor groove, are shown in red.

with the 3′-terminal sugar-phosphate backbone at $C^{75}A^{76}$. This network of interactions is completely disrupted in the unliganded enzyme, and the entire DNF surface loop spanning amino acids 64–76 (bridging β2 and αC; Figure 4) adopts a different conformation (Figures 3A and 5A). This loop is less well ordered in the unliganded enzyme, such that Val71 as well as a number of side chains could not be modeled. Some of the intramolecular contacts between this DNF loop and the ABD surface loop spanning residues 195–204 are also altered, although a significant interface between these two peptides is preserved in the structural transition.

The conformational change in the DNF 64–76 loop upon tRNA binding has at least two important consequences. First, the side chain of Asp66 is reoriented to point into the glutamine binding pocket, where it makes ionic contacts with both the substrate α amino group and the His215 imidazole (Figure 5B). Second, new internal structuring contacts are made by the side chain of Glu73, which is disordered in the unliganded enzyme. In the tRNA complex, the reoriented Glu73 carboxylate is positioned within close hydrogen bonding distance of the Glu34 carboxylate in the ATP binding site and is also stabilized by hydrophobic interactions with Pro35. In turn, a local rearrangement of the ATP binding cleft spanning amino acids Pro32-Pro33-Glu34-Pro35 also occurs, with new intramolecular contacts formed between Pro35-Asp74 and Pro33-Asp66. Displacement of Glu34 away from its position in the unliganded enzyme is also required to accommodate the A76 ribose group, while the 1–2 Å movements of the polypeptide backbone at residues 32–35 create a more complementary interface for binding ATP (Figure 5B).

The ABD rotation also stabilizes a distal section of the active site cleft that binds the side chain of glutamine. The side chain of Tyr211, located directly after the ABD in a flexible portion of polypeptide chain, is rotated more deeply into the pocket. This positions it to make a direct hydrogen bond with the glutamine amide (Figure 5B). In addition, the adjacent side chains of Cys229, Arg30, and His215 also undergo small rearrangements and are stabilized in the tRNA-bound complexes. The change in position of the Tyr211 side chain is directly facilitated by stacking interactions with Phe233 and with the 3′-terminal adenine ring of the tRNA. Thus, the ABD rotation generates a complementary protein surface that provides interactions with both main chain and side chain portions of the amino acid ligand.

The two separate halves of the DNF appear to form a single rigid unit when the superposition is performed with backbone atoms within DNF core regions (Figures 1B and 3A). However, superposition of the ABD backbones reveals that α helices G and H from the second half of the fold actually track much more closely with this inserted domain than with the DNF. Figure 3B shows that these two helices directly adjacent to the ABD largely maintain their interface with each other and with the ABD when tRNA binds, while the remainder of the DNF (consisting of the five strands β1, β2, β3, β9, and β10 and the two helices αB and αC) is rotated away by 10°. The axis of rotation between the DNF and ABD passes approximately parallel, and very close, to αG and αH, accounting for why these helices can be superimposed reasonably well with either rigid-body domain. The consequence of this architecture is to separate both glutamine and $tRNA^{Gln}$ binding elements away from the β1-turn-αB motif, which forms the platform for ATP bind-

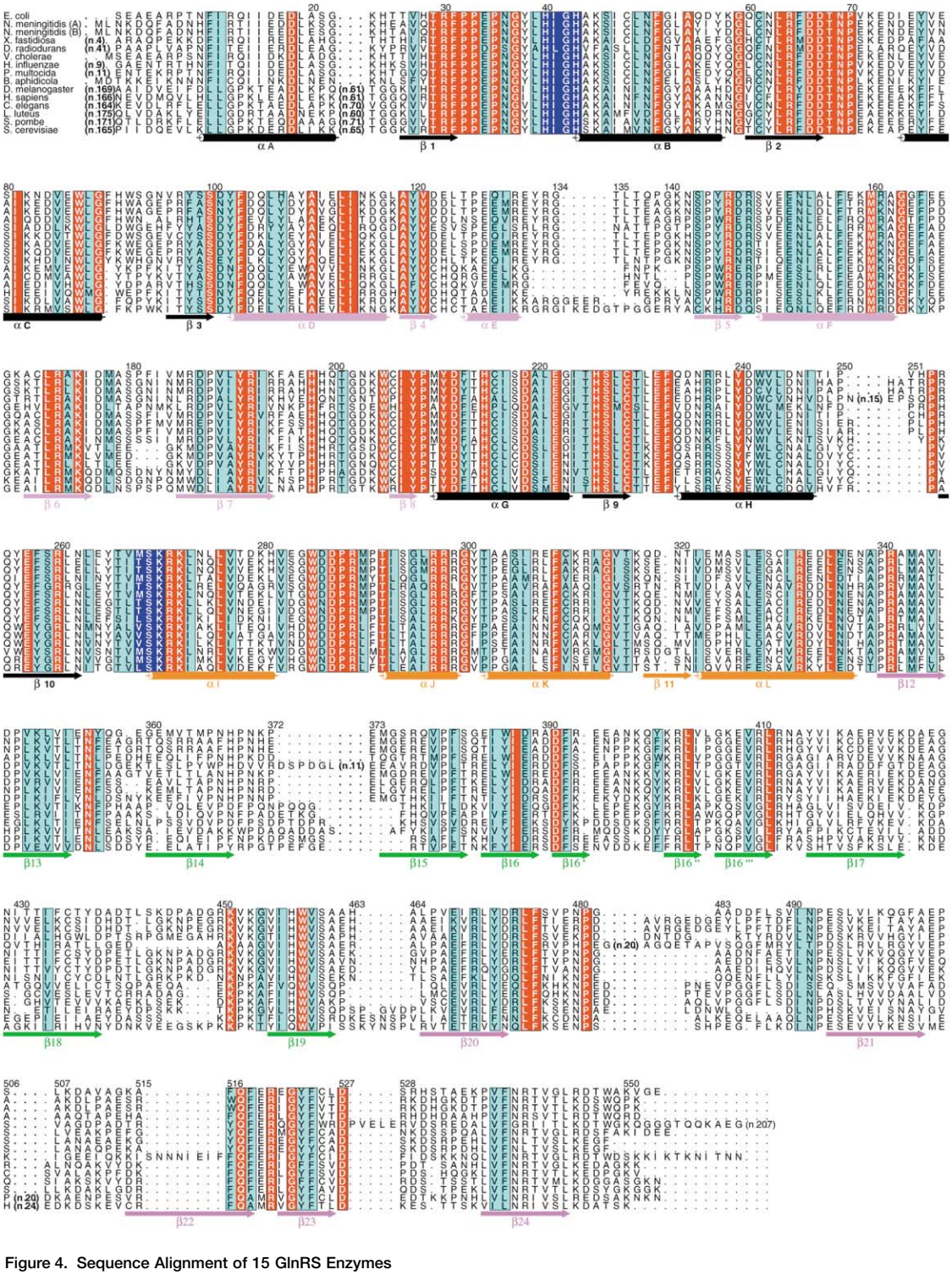

Figure 4. Sequence Alignment of 15 GlnRS Enzymes

Strictly conserved amino acids are boxed in red, highly conserved regions are boxed in light blue, and the "HIGH" and "MSK" signature motifs characteristic of class I tRNA synthetases are boxed in dark blue. Secondary structure elements derived from the *E. coli* structure are indicated under the alignment and are color-coded by domain as in Figure 1.

ing. The N terminus of αH points directly into the minor groove of the tRNA acceptor stem, where Asp235 makes direct and water-mediated interactions with the bases of G2 and G3 [35]. Directly adjacent to αH, two loops of the ABD also penetrate the acceptor end to recognize the G2-C71 pair and to facilitate melting of U1-A72 ([6]; Figure 3B). Thus, these three tRNA binding peptides, all of which are crucial to specific recognition of acceptor-end identity nucleotides at G73, U1-A72, G2-C71, and G3-C70 [26], reorient as a single unit toward the ATP

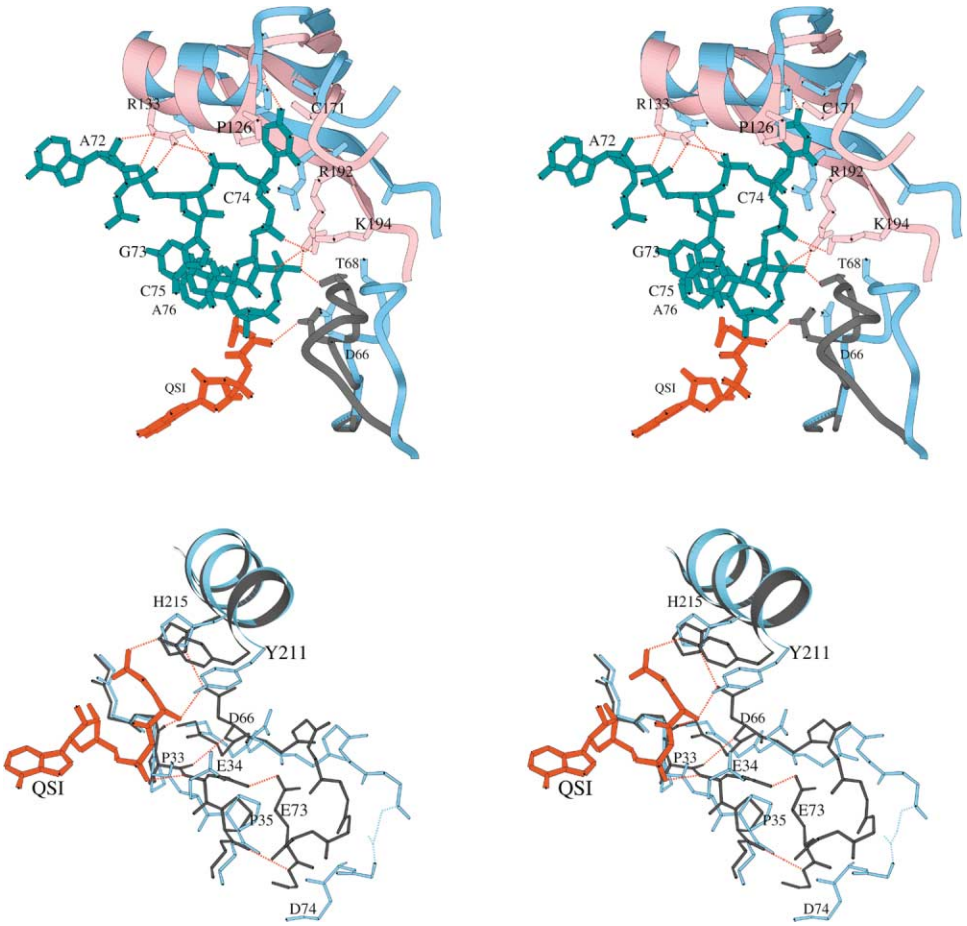

Figure 5. Substrate Juxtaposition by Induced Fit

(A) Stereo view of enzyme conformational changes in the vicinity of the tRNA 3′-end. The tRNA-bound and unliganded enzymes are superimposed on the basis of equivalent residues in the DNF domains (see text). tRNA, dark blue; unliganded enzyme, light blue; complexed enzyme, gray (DNF domain) and pink (ABD). Dotted red lines indicate hydrogen bonds observed in the GlnRS-tRNA complex. QSI inhibitor from the complexed structure, red.

(B) Stereo view of enzyme conformational changes in the active site, with structures superimposed as in (A). Complexed enzyme, gray; unliganded enzyme, blue; QSI inhibitor, red. The disorder in the surface loop at Val71 in the unliganded enzyme is shown by the dotted blue line (right). Dotted red lines indicate hydrogen bonds observed in the GlnRS-tRNA complex.

binding β sheet core of the DNF when tRNA binds. Similarly, Tyr211, His215, Cys229, Phe233, and other amino acids from αG and αH are major determinants forming the glutamine binding pocket. The rotation of αG and αH as part of a rigid structural unit including the ABD thus assembles the glutamine binding pocket concomitantly with binding of the tRNA acceptor end.

In vivo genetics and/or in vitro mutagenesis supports important roles in catalysis and/or tRNA discrimination for Asp66, Ile129, Arg130, Glu131, Leu136, Tyr211, Phe233, and Asp235, all of which are located within the DNF and ABD [33, 35–39]. Each of these amino acids directly binds, or is immediately adjacent to, the glutamine or tRNA substrates. The unliganded structure now also reveals the importance of additional residues that are likely required to mediate the conformational changes, rather than to bind ligands directly.

Anticodon Binding and Helical Subdomains

Like the tRNA-bound structure, the carboxy-terminal anticodon binding β barrel domains of unliganded GlnRS (ACB) are less well ordered than the DNF domain and the ABD, as judged by higher B factors and higher rms deviation between the two independently determined unbound models (Figure 2A). Nonetheless, a core unit comprising all six β strands of the proximal barrel together with the three most closely adjoining strands of the distal β barrel is very similar in the presence and absence of tRNA. In these segments the backbone atoms of 86 amino acids superimpose with an rms deviation in equivalent positions of just 0.40 Å. These regions are also the most similar portions of the β barrels between the two unliganded models. The inclusion of peptides from both β barrels in this superposition shows that these domains do not exhibit independent flexibility upon tRNA binding but, instead, reorient as a single rigid body with respect to the position of the DNF.

This superposition reveals a subtle, but significant, global repositioning of the ACB and DNF domains upon tRNA binding, with core structural elements of the ACB uniformly displaced outward by approximately 1 Å (corresponding to about 4° rotation) to accommodate the anticodon stem loop (Figures 1B and 6A). Interestingly,

there are at most only small local changes in the amino acids making up the binding pockets for the C34, U35, and G36 bases, which are largely preformed in the unliganded enzyme. However, a number of the more mobile segments of the ACB are positioned near the anticodon, including surface loops adjacent to U35 (amino acids His368–Asn370) and G36 (amino acids Gln399–Arg402), the partly disordered C-terminal amino acid segment Val542–Glu553, and the disordered surface loop at amino acids 443–454. At these positions the two unliganded models and the tRNA-bound structure diverge with rms deviations of 1–2 Å, so that small induced-fit rearrangements of this magnitude may occur. Alternatively, the unliganded enzyme may sample the tRNA-bound structure as one conformer, which is significantly populated in solution. It is of interest that GlnRS makes discriminatory hydrogen bonds with all three of the Watson-Crick moieties of C34 [19], so that accommodation of the ^{mnm5s2}UUG anticodon apparently requires a different conformation than CUG. The flexible C-terminal peptide, together with the adjacent disordered surface loop, may play a role in reconfiguring the wobble-base pocket when the modified U34 replaces C34.

A larger structural change in GlnRS is associated with binding to the central globular portion of the tRNA. At the extreme inner corner of the tRNA L shape, a β strand and surface loop forming part of the helical subdomain (inner corner loop [ICL]) adopt a different and somewhat less well-ordered conformation in the absence of tRNA (Figure 6A). The ICL is conserved in class I tRNA synthetases; in GlnRS, genetic studies have shown that Lys317 and Gln318 in the loop mediate communication from the anticodon [31]. When tRNA binds, the 11 amino acids of the ICL (Arg312–Ile322, comprising β11 and the C-terminal portion of αK) reorient up to 7–8 Å toward the body of the enzyme, while forming an extensive network of contacts to the sugar-phosphate backbone at nucleotides U6–U8 and C11–A14. Further, the ICL also makes new internal packing contacts with three other enzyme segments. These comprise amino acids near the N terminus (Thr8–Ile11), a section of α helix B (amino acids Lys45–Leu49) within the first half of the DNF, and strand β10 in the second half of the DNF (residues Arg254–Asn262). Significantly, Arg260 and Leu261 bind ATP, and the contacted segments are also adjacent to the conserved ^{40}HIGH and ^{268}MSK active site motifs. This rearrangement upon tRNA binding thus provides a direct pathway to influence the conformation of the active site.

Superposition on the DNFs shows that amino acids Arg260-Leu261-Asn262 are significantly displaced as a direct consequence of the ICL reorientation upon tRNA binding (Figure 6B). This changes the position of both the Arg260 β carbon and the Leu261 main chain carbonyl oxygen with respect to the DNF core. The Arg260 side chain is disordered in the unliganded enzyme but makes direct and solvent-mediated contacts to ATP in the ternary GlnRS-tRNA-ATP complex. tRNA binding also recruits Glu232 to form an ion pair with Arg260, helping to stabilize its position over the adenine ring. Similarly, the Leu261 main chain carbonyl oxygen accepts a hydrogen bond from the exocyclic $^{6}NH_2$ moiety of adenine, helping to provide specificity for ATP. Thus, the movement of β10 creates a key complementary portion of the ATP binding site. The importance of Arg260 has been established by mutagenesis [40].

A sizable portion of the helical subdomain (residues 263–337) is also displaced with respect to the DNF (Figure 6). Asn262 is followed directly by a surface loop containing the ^{268}MSK conserved class I motif. Following Lys270 in sequence is an irregular region consisting of three α helices (αI, αJ, and αK), the β11 strand at the tRNA inner corner, and the long αL helix bridging to the ACB region. Of these elements, the N-terminal portion of both αK and αL superimpose precisely with the DNF core, despite being connected by the flexible ICL (Figure 6A). However, the MSK loop, αJ, and αK are each significantly displaced. The displacement extends to include a very large loop emanating from the proximal anticodon binding β barrel (amino acids 471–496), which packs on the front face of the helical subdomain. The movement of this loop is facilitated by flexibility in its connection to the β barrel core, as revealed by separate superpositions of the ACB domains (Figure 6A).

The interface between the proximal β barrel loop and helical subdomain is maintained when tRNA binds, except for a more flexible section comprising amino acids Ala483–Ser489 at the tip of the loop. This peptide adopts significantly different conformations in the two unliganded models, as does the segment spanning Val267–Leu273. However, comparison of these structures with the tRNA-bound model shows that the backbone at, and adjacent to, Lys270 bends sharply inwards only in the latter structure. Although the Lys270 side chain is disordered in the unliganded enzyme, its backbone position is displaced by about 3 Å away from the ATP binding site (Figure 6B). Moreover, the Lys270 side chain must adopt an extended conformation in the cocrystals in order to reach the ATP α-phosphate. Thus, ATP and/or tRNA binding are required to reorient the MSK loop for catalysis of the aminoacylation reaction.

Comparison of these models also identifies several interdomain contacts specific to the tRNA-bound state, which may be crucial to stabilizing the active site conformation. Significantly, key interactions of the MSK sequence with the DNF domain are present only in the tRNA-bound structure (Figure 6B). These include hydrogen bonds between the Met268 backbone carbonyl and the His40 imidazole ring and between the side chains of Lys270 and Asn36. Additionally, an adjacent well-defined hydrophobic stacking interaction between Tyr38 and Trp285 appears to be destabilized in the unliganded enzyme. As described above, the peptide spanning residues Pro32–Pro35 is also rearranged in the ligand binding transition as a consequence of new contacts with the DNF loop spanning residues 64–76 (Figure 5B). Thus, induced conformational transitions apparently arising from enzyme contact with different parts of the tRNA converge to influence the structure and interactions in the ATP binding site.

An unexpected feature of the unliganded structure is the presence of a disulfide bond linking Cys48 of the DNF to Cys310 of the helical subdomain. These two sulfurs are positioned 3.6 Å apart in the tRNA-bound enzyme and are brought into proximity for covalent bond formation by a 1–2 Å relative movement of the αB and αK backbones. In both unliganded models the electron

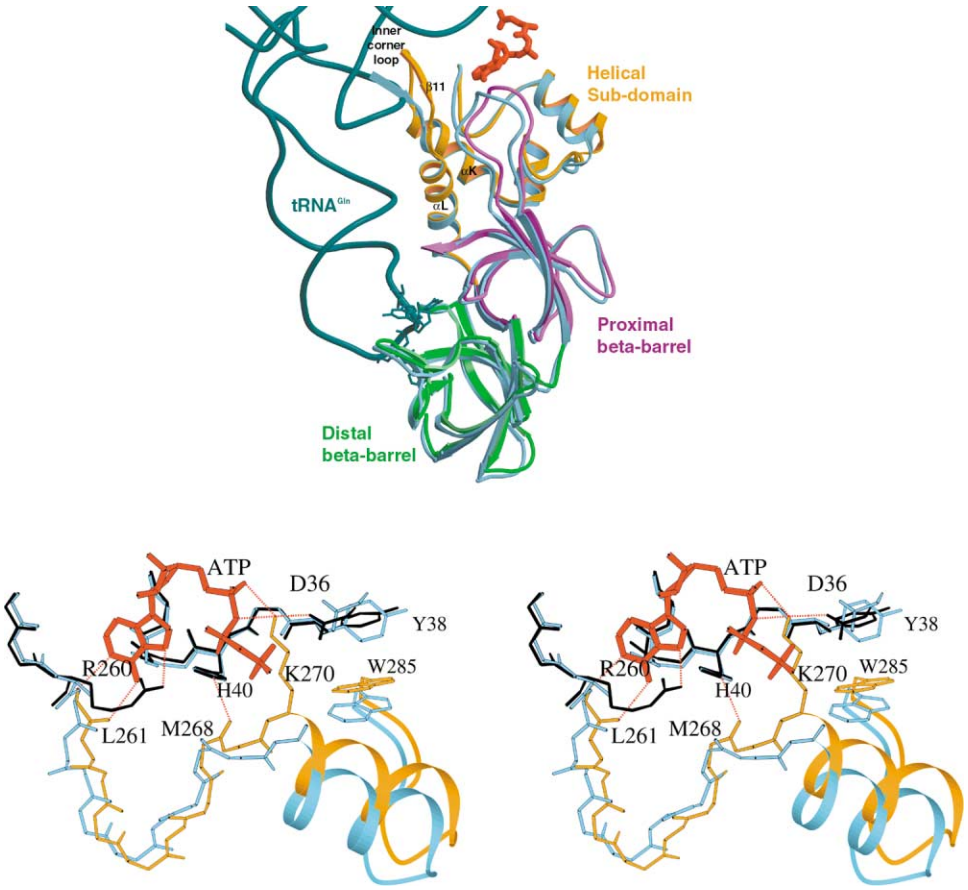

Figure 6. Long-Range Communication in the GlnRS-tRNA Complex

(A) Superposition of the complexed and unliganded GlnRS structures based on atoms of the DNF and showing conformational changes in the C-terminal portion of the enzyme. Unliganded enzyme, blue; complexed enzyme, color-coded as in Figure 1. Anticodon nucleotides, dark blue. The movement of the large connecting loop in the proximal β barrel domain (magenta) tracks with movements of portions of the helical subdomain (orange).

(B) Stereo view of enzyme conformational changes in the active site. Color-coding of unliganded and complexed enzymes is as in previous figures. Dotted red lines indicate hydrogen bonds observed in the GlnRS-tRNA-ATP complex. The superposition is on atoms of the DNF domain.

density demonstrating the covalent bond is strong and unambiguous, while tRNA cocrystal structures determined concurrently from the same enzyme preparation stored in the presence of DTT consistently show reduced cysteines, as expected for intracellular *E. coli* proteins and as also observed in all previous GlnRS-$tRNA^{Gln}$ crystals. Cys48 and Cys310 are conserved in five of nine bacterial GlnRS species for which sequences are available but are not present in any eukaryotic enzyme. GlnRS activity in vitro was unaffected by incubation with oxidized glutathione in the presence of a molar excess of the redox protein DsbA, conditions which are strongly oxidizing (data not shown). Thus, the functional significance of this disulfide bond, if any, is unknown.

Discussion

GlnRS Architecture and Structure-Function Relationships

The comparison of tRNA-bound and unliganded GlnRS structures reveals a complex protein architecture, consisting of interspersed rigid and flexible segments, which, together, facilitate the conformational transitions required to bind and properly juxtapose reactive moieties of the three substrates. The two halves of the DNF maintain their relationship during ligand binding, but flexibility within this domain is built in at the interface of helices αG and αH with the parallel β sheet core (Figure 3B). At this interface, small movements spread over a large contact area divide these two helices from the remainder of the DNF, allowing them to move in concert with the ABD. Four surface peptide segments within the large DNF and ABD/αGαH domains (amino acids Pro32–Pro35, Arg64–Glu76, Thr135–Gly140, and Phe195–Lys204) then reorient independently of the larger motions, generating portions of the complementary interfaces with the tRNA acceptor end and with glutamine. The C-terminal β barrels preserve their structural relationship with each other and rotate slightly outward as a single unit to accommodate the tRNA anticodon (Figure 6A). The large loop connecting strands β20 and β21 of the proximal barrel reorients separately from

the C-terminal domains, moving instead with peptides from the central helical subdomain, on which it packs. The origin of the movements in the helical subdomain appears to be reorientation of the ICL upon binding the inner corner of the tRNA. The extensive backbone contacts in this region may help drive this rearrangement, which produces improved interdomain packing with the DNF and further positioning of side chains, which bind ATP (Figure 6B). Thus, it appears that the ATP and glutamine binding sites are assembled as a consequence of structural rearrangements converging from the acceptor end and the inner corner of the L shape, each toward the centrally positioned active site (Figures 5 and 6B).

These rearrangements in GlnRS upon ligand binding are consistent with fluorescence and neutron scattering experiments, which revealed the presence of conformational changes in solution [23–25]. In particular, the neutron scattering data showed that the overall dimensions of the enzyme are largely maintained, as significant differences were observed mainly in the high-angle region—indicative of local rearrangements, but not large-scale changes [23].

The structural changes also explain the requirement for tRNA binding prior to catalysis of glutaminyl adenylate formation [41], a feature shared with GluRS, ArgRS, and class I LysRS [30]. In GlnRS, it is clear that neither the ATP nor the glutamine binding sites are fully formed in the unliganded enzyme. Because rearrangements occur throughout the structure, it seems highly likely that they are specifically generated by tRNA binding. Indeed, a requirement for global tRNA-enzyme interaction to induce active site formation was also suggested by kinetic studies on human GlnRS [42]. The observation that enzyme-tRNA complexes bound to ATP, AMP, QSI, or AMPCPP/amino acid each adopt identical quaternary conformations also suggests the primary role of the tRNA [6, 20, 21, 34]. However, the absence of binary GlnRS-tRNA or GlnRS-ATP structures for direct comparison leaves some ambiguity in this respect. Moreover, other experiments suggest that intermediate ligand-induced conformational states may exist. For example, fluorescence titrations suggest that either ATP or tRNA binding alone can induce an enzyme conformational change [24]. Further, crystals of the GlnRS-tRNA complex do not grow in the absence of the smaller ligands, suggesting that these are required for part of the induced fit. Additionally, diffraction of the unliganded crystals deteriorates severely when glutamine is soaked in, and the crystals do not form if glutamine is included in the mother liquor. While the latter observation suggests a binding interaction between glutamine and the unliganded enzyme, the kinetic order (or randomness) of substrate addition in the steady-state pathway has not yet been established. Thus, we suggest that the unliganded and the ternary/quaternary complexes compared herein likely represent the two extreme structural states of GlnRS and that complexes with fewer bound substrates may adopt intermediate conformations. Clearly, additional kinetic and crystallographic analyses are required for a full description of the induced-fit pathway.

These structural comparisons also help interpret numerous mutational studies, which implicated specific amino acids and peptide segments in communication pathways between the active site and distal regions of the complex. In particular, the structure supports the hypothesis, made on the basis of genetic data, that ICL binding at the inner corner of the tRNA is involved in signal transduction [31]. The apparent propagation of structural changes from the ICL to the directly adjacent ATP binding site indeed suggests that binding at this position is coupled to active site assembly. This also provides an explanation for how tRNA mutations in the globular core region (adjacent to the inner corner) can have strong effects on k_{cat} [28, 29]. However, the long αL helix connecting the ICL to the anticodon maintains its orientation with respect to the DNF. Therefore, it appears that recognition of anticodon identity nucleotides U35 and G36 [26, 27], as well as coupling between anticodon recognition and glutamine binding [27, 29], may instead be communicated through the large loop spanning β20 and β21 of the proximal barrel. The importance of this large loop has also been suggested on the basis of genetic data [32]. Anticodon binding does generate a small movement inward of the two β barrels, which might trigger the reorientation of the large loop. Alternatively or additionally, this reorientation might arise by structural transmission from the ICL. Further well-designed mutational experiments, coupled to structural analysis, should be helpful in further elucidating the importance of the two pathways.

Although the large proximal barrel loop does reorient upon tRNA binding, the precise manner by which this might be triggered by recognition of identity anticodon nucleotides (U/C34, U35, and G36) is not evident. Comparison of the tRNA-bound and unliganded structures does not show specific, clear rearrangements in response to binding of the bases. Instead, numerous peptide segments adjacent to the anticodon are quite flexible (as revealed by high thermal factors and significant deviation between the two unliganded models) or fully disordered in both states. It is not clear why the presence of a noncognate anticodon nucleotide, for example, could not be accommodated by local rearrangements while preserving the small inward movement of the two domains and the proximal barrel loop movement (Figure 6A). This ambiguity is in contrast to the much clearer interpretations that can be offered for tRNA acceptor-end binding, where the ABD/αGαH rotation is clearly coupled to specific recognition of bases and to stabilization of the otherwise unfavorable hairpin (Figure 3B). In that case it is evident that the unliganded enzyme does not adopt the required conformation, which is a function of both DNF and ABD sequences and requires their precise ligand-induced juxtaposition.

Induced-Fit Rearrangements in Class I tRNA Synthetases

The conformational changes described for GlnRS on the path from the unliganded enzyme toward the tRNA complex are a clear example of induced fit in protein-RNA interactions. Although induced fit necessarily incurs an entropic penalty compared with a preformed and rigid enzyme, the built-in flexibility may nonetheless

increase the kinetic association rate, thus lowering the free-energy barrier for complex formation [43, 44]. A mechanism for this could be that the fraction of productive initial enzyme-substrate contacts increases when a capacity for rearrangement of the initial "encounter complex" exists in one or both partners. In a different sense, induced fit also represents an underlying mechanism that provides specificity for the amino acid or tRNA [45]. In a noncognate complex with either substrate, the induced conformational changes may differ or else may represent only a subset of those that occur when glutamine or $tRNA^{Gln}$ binds. As a consequence, the catalytic groups of noncognate substrates in the final quaternary complex could be misaligned with respect to each other, resulting in decreased rates for the chemical steps of aminoacyl adenylate and aminoacyl-tRNA formation.

It is of interest to examine the alignment of GlnRS sequences with respect to the structural transitions and tRNA interactions (Figure 4). This shows that the DNF, ABD, and helical subdomains are much better conserved than the C-terminal β barrels. While many of the amino acids directly recognizing the anticodon nucleotides are well conserved, less conservation is evident in residues making or facilitating specific contacts at the acceptor end, such as Asp235, Pro181, or Leu136 (Figure 3B). This suggests an evolutionary divergence in the importance or nature of the tRNA identity nucleotides at positions 73, 1–72, 2–71, or 3–70 [26]. With respect to the induced-fit transitions, many of the amino acids involved in the new intramolecular ABD-DNF contacts or 3′-end backbone contacts when tRNA binds are well conserved (Figure 5), as are the intersubunit interactions between the helical subdomain and DNF (Figure 6B). However, neither the ICL sequence nor that of the central portion of the proximal β barrel hairpin (which packs directly on the helical subdomain) is conserved. These observations suggest that most local active site rearrangements may have been retained through evolutionary time but that at least some aspects of the long-distance pathways for communication from the tRNA core region and the anticodon stem loop have instead diverged.

All class I tRNA synthetases retain the Rossman active site fold as well as a similar global tertiary relationship among the DNF, ABD, and helical subdomains. However, within this common tertiary organization there is considerable divergence in the detailed structures of the domains, including the presence of sizable insertions in some enzymes. Despite this, a common feature emerging from comparisons of tRNA-bound and unbound states in GlnRS, GluRS, ArgRS, and TyrRS is that the domain reorientations are consistently small, on the order of those described here for GlnRS [14, 15, 17]. By contrast, a large 47° rotation of the ABD with respect to the DNF accompanies tRNA binding to IleRS [7]. Thus, large reorientations may be a unique feature of the editing class I tRNA synthetases (IleRS, ValRS, and LeuRS). Other, more detailed features of the conformational changes are likely to be idiosyncratic to each system. For example, the DNF in TrpRS also alters its internal structure upon ligand binding [16], but the structural split occurs between the most N-terminal α helix and the remainder of the fold, rather than within the second half of the fold as in GlnRS (Figure 3B).

At this time, comparison of the mechanisms used by those class I tRNA synthetases that require tRNA for aminoacyl adenylate formation—GlnRS, GluRS, ArgRS, and class I LysRS—is still premature, because the sets of structures available in each system do not correspond to the same liganded states. Although significant insight into this question is now in hand for GlnRS and ArgRS [14], further structures and kinetic data are clearly needed in both cases. The requirement for a full set of structures together with knowledge of the steady-state kinetic pathway highlights the complex nature of the mechanisms used to maintain fidelity of information transfer by this ancient family of enzymes.

Biological Implications

Specificity in expression of the universal genetic code is largely determined by the ability of aminoacyl-tRNA synthetases to accurately discriminate among amino acids and tRNAs. The structural mechanisms by which this specificity arises are thus of fundamental significance to understanding information transfer processes in all organisms. Here, we describe a set of structural transitions in *Escherichia coli* GlnRS, which show how ligand binding is coupled to assembly of a catalytically proficient active site. Strong sequence similarities among GlnRS enzymes in the prokaryotic and eukaryotic domains indicate that findings are general across nature (Figure 4). Recent data showing the involvement of tRNA synthetases in RNA splicing, amino acid biosynthesis, and cellular apoptosis underscore the importance of this enzyme family in processes previously thought to be unrelated to translation [18].

E. coli GlnRS has long served as a model system for the investigation of themes in complex RNA-protein interactions [6, 22, 36, 46]. This unliganded structure can thus be compared with the previously determined tRNA-bound complexes, and the deduced induced-fit rearrangements can then be integrated with a wealth of genetic and biochemical information. For example, the long-established requirement of tRNA binding for synthesis of glutaminyl adenylate is now seen to arise because flexible active site peptides are improperly juxtaposed in the absence of ligands. Pathways by which information in the tRNA core and anticodon is signaled to the catalytic center are shown to involve rearrangement of a key surface loop previously implicated by genetic selections, which binds at the inner corner of the tRNA L shape. Finally, the comparison of unliganded and tRNA-bound structures shows how the construction of tRNA and amino acid binding sites are mutually interdependent. This finding suggests that reengineering of GlnRS for expansion of the genetic code repertoire will likely require amino acid replacements far from the active site.

Experimental Procedures

Glutaminyl-tRNA synthetase was purified and stored at 20–25 mg/ml as described [46, 47]. Enzyme was dialyzed into a solution containing 10 mM PIPES (pH 7.5) and 10 mM β-mercaptoethanol, and the ATP analog AMPCPP was added to a concentration of 5 mM. Some crystals were grown in the presence of 5 mM ATP in place of AMPCPP. The concentration of enzyme was 100 μM. The GlnRS-

AMPCPP complex was then mixed at a 1:1 volume ratio with mother liquor, and crystals were grown by hanging drop vapor diffusion at 290 K (see Table 1 for growth conditions). Microseeding with initially obtained small crystals as seed stock slightly accelerated growth and increased the occurrence of suitably sized crystals for data collection.

Crystals used for data sets 2 and 3 were taken directly from the crystallization solution and mounted in a cryoloop under a stream of nitrogen at 100 K. Crystals for data set 1, which grew under slightly different conditions and showed improved diffraction to 2.4 Å resolution (Table 1), were transferred from drops into a solution containing 5 mM AMPCPP, 20% PEG 1000, 10% PEG 8000, 0.1 M sodium acetate, and 0.1 M PIPES (pH 7.5), prior to mounting in a cryoloop under a nitrogen stream at 100 K.

All data were reduced with MOSFLM and the CCP4 suite of programs (Table 1; CCP4, 1994). The structure was first solved to 2.65 Å resolution by molecular replacement with CNS [48], with tRNA-bound glutaminyl-tRNA synthetase as a search model and observed amplitudes from data set 2 ([21]; Table 1). Indexing and examination of systematic absences revealed a solution in either space group $P222_1$ or $P2_12_12_1$. The initial rotational search revealed an equivalent solution for both spacegroups, and the translational search showed a clear solution in space group $P2_12_12_1$ with a correlation coefficient of 31%. A set of five individual fragments was used for rigid-body refinement in CNS, resulting in an initial R factor of 46%. At this juncture model building and refinement with $F_o - F_c$ and $2F_o - F_c$ density maps as a guide failed to reduce R_{free}. However, refinement proceeded smoothly after the data were local scaled to data set 3, with a scaling neighborhood of ten reflections. Rounds of refinement and extensive manual rebuilding, including overall anisotropic B factor refinement and application of bulk solvent corrections, resulted in a final R_{free} of 31% (Table 1). There is one GlnRS monomer in the asymmetric unit.

The unliganded GlnRS structure was also solved independently in the same lattice with a different set of data to 2.4 Å resolution (data set 1). Molecular replacement in CNS, as described above, produced a translational correlation coefficient of 34.5 % in space group $P2_12_12_1$. Refinement was performed as above, resulting in a final R factor of 24.5 % and an R_{free} of 33.4%. Local scaling against either data set 2 or 3, followed by continued refinement against the scaled amplitudes, did not further lower R_{free} in this case. For each structure the somewhat high R_{free} value likely arises, at least in part, from the intrinsically high mobility.

Model building was performed with the program O [49]. Rigid-body movements were analyzed with the PSHIF module of the TOP program package [50].

Acknowledgments

This work was supported by National Institutes of Health award GM63713 (to J.J.P.). Portions of this research were also performed at the Stanford Synchrotron Radiation Laboratory, a national user facility operated by Stanford University on behalf of the U.S. Department of Energy, Office of Basic Energy Sciences. The SSRL Structural Molecular Biology Program is supported by the Department of Energy, Office of Biological and Environmental Research, and by the National Institutes of Health, National Center for Research Resources, Biomedical Technology Program, and the National Institute of General Medical Sciences.

Received: December 16, 2002
Revised: March 4, 2003
Accepted: March 7, 2003
Published: May 6, 2003

References

1. Ibba, M., and Söll, D. (2000). Aminoacyl-tRNA synthesis. Annu. Rev. Biochem. *69*, 617–650.
2. Eriani, G., Delarue, M., Poch, O., Gangloff, J., and Moras, D. (1990). Partition of tRNA synthetases into two classes based on mutually exclusive sets of sequence motifs. Nature *347*, 203–206.
3. Nagel, G.M., and Doolittle, R.F. (1995). Phylogenetic analysis of the aminoacyl-tRNA synthetases. J. Mol. Evol. *40*, 487–498.
4. Schimmel, P., and Ribas de Pouplana, L. (2001). Formation of two classes of tRNA synthetases in relation to editing functions and genetic code. Cold Spring Harb. Symp. Quant. Biol. *66*, 161–166.
5. Brick, P., Bhat, T.N., and Blow, D.M. (1989). Structure of tyrosyl-tRNA synthetase refined at 2.3 Å resolution. Interaction of the enzyme with the tyrosyl adenylate intermediate. J. Mol. Biol. *208*, 83–98.
6. Rould, M.A., Perona, J.J., Söll, D., and Steitz, T.A. (1989). Structure of *E. coli* glutaminyl-tRNA synthetase complexed with $tRNA^{Gln}$ and ATP at 2.8 Å resolution. Science *246*, 1135–1142.
7. Silvian, L.F., Wang, J., and Steitz, T.A. (1999). Insights into editing from an Ile-tRNA synthetase structure with tRNAIle and mupirocin. Science *285*, 1074–1077.
8. Sugiura, I., Nureki, O., Ugaji-Yoshikawa, Y., Kuwabara, S., Shimada, A., Tateno, M., Lorber, B., Giege, R., Moras, D., Yokoyama, S., et al. (2000). The 2.0 Å crystal structure of *Thermus thermophilus* methionyl-tRNA synthetase reveals two RNA-binding modules. Structure *8*, 197–208.
9. Fukai, S., Nureki, O., Sekine, S., Shimada, A., Tao, J., Vassylyev, D.G., and Yokoyama, S. (2000). Structural basis for double-sieve discrimnation of L-valine from L-isoleucine and L-threonine by the complex of $tRNA^{Val}$ and valyl-tRNA synthetase. Cell *103*, 793–803.
10. Cusack, S., Yaremchuk, A., and Tukalo, M. (2000). The 2 Å crystal structure of leucyl-tRNA synthetase and its complex with a leucyl-adenylate analogue. EMBO J. *19*, 2351–2361.
11. Perona, J.J., Rould, M.A., Steitz, T.A., Risler, J.-L., Zelwer, C., and Brunie, S. (1991). Structural similarities in glutaminyl and methionyl-tRNA synthetases suggest a common overall orientation of tRNA binding. Proc. Natl. Acad. Sci. USA *88*, 2903–2907.
12. Newberry, K., Hou, Y.-M., and Perona, J.J. (2002). Structural origins of amino acid selection without editing by cysteinyl-tRNA synthetase. EMBO J. *21*, 2778–2787.
13. Serre, L., Verdon, G., Choinowski, T., Hervouet, N., Risler, J.-L., and Zelwer, C. (2001). How methionyl-tRNA synthetase creates its amino acid recognition pocket upon L-methionine binding. J. Mol. Biol. *306*, 863–876.
14. Delagoutte, B., Moras, D., and Cavarelli, J. (2000). tRNA aminoacylation by arginyl-tRNA synthetase: induced conformations during substrates binding. EMBO J. *19*, 5599–5610.
15. Yaremchuk, A., Kriklivyi, I., Tukalo, M., and Cusack, S. (2002). Class I tyrosyl-tRNA synthetase has a class II mode of cognate tRNA recognition. EMBO J. *21*, 3829–3840.
16. Ilyin, V.A., Temple, B., Hu, M., Li, G., Yin, Y., Vachette, P., and Carter, C.W., Jr. (2000). 2.9 Å crystal structure of ligand-free tryptophanyl-tRNA synthetase: domain movements fragment the adenine nucleotide binding site. Protein Sci. *9*, 218–231.
17. Sekine, S., Nureki, O., Shimada, A., Vassylyev, D.G., and Yokoyama, S. (2001). Structural basis for anticodon recognition by discriminating glutamyl-tRNA synthetase. Nat. Struct. Biol. *8*, 203–206.
18. Ibba, M., and Söll, D. (2001). The renaissance of aminoacyl-tRNA synthesis. EMBO Rep. *2*, 382–387.
19. Rould, M.A., Perona, J.J., and Steitz, T.A. (1991). Structural basis of anticodon loop recognition by glutaminyl-tRNA synthetase. Nature *352*, 213–218.
20. Perona, J.J., Rould, M.A., and Steitz, T.A. (1993). Structural basis for transfer RNA aminoacylation by *E. coli* glutaminyl-tRNA synthetase. Biochemistry *32*, 8758–8771.
21. Rath, V.L., Silvian, L.F., Beijer, B., Sproat, B.S., and Steitz, T.A. (1998). How glutaminyl-tRNA synthetase selects glutamine. Structure *6*, 439–449.
22. Perona, J.J. (2003). Glutaminyl-tRNA synthetase. In The Aminoacyl-tRNA Synthetases, M. Ibba, C. Francklyn, and S. Cusack, eds. (Georgetown, TX: Landes Bioscience), in press.
23. Perona, J.J. (1990). Crystal structure of the *E. coli* glutaminyl-tRNA synthetase:$tRNA^{Gln}$ complex. PhD thesis, Yale University, New Haven, Connecticut.
24. Bhattacharyya, T., and Roy, S. (1993). A fluorescence spectroscopic study of substrate-induced conformational changes in glutaminyl-tRNA synthetase. Biochemistry *32*, 9268–9273.

25. Mandal, A.K., Bhattacharyya, A., Bhattacharyya, S., Bhattacharyya, T., and Roy, S. (1998). A cognate tRNA specific conformational change in glutaminyl-tRNA synthetase and its implication for specificity. Protein Sci. *7*, 1046–1051.
26. Jahn, M., Rogers, M.J., and Söll, D. (1991). Anticodon and acceptor stem nucleotides in $tRNA^{Gln}$ are major recognition elements for *E. coli* glutaminyl-tRNA synthetase. Nature *352*, 258–260.
27. Ibba, M., Hong, K.-W., Sherman, J.M., Sever, S., and Söll, D. (1996). Interactions between tRNA identity nucleotides and their recognition sites in glutaminyl-tRNA synthetase determine the cognate amino acid affinity of the enzyme. Proc. Natl. Acad. Sci. USA *93*, 6953–6958.
28. Nissan, T.A., Oliphant, B., and Perona, J.J. (1999). An engineered class I transfer RNA with a class II tertiary fold. RNA *5*, 434–445.
29. Nissan, T.A., and Perona, J.J. (2000). Alternative designs for construction of the class II transfer RNA tertiary core. RNA *6*, 1585–1596.
30. Ibba, M., Becker, H.D., Stathopoulos, C., Tumbula, D.L., and Söll, D. (2000). The adaptor hypothesis revisited. Trends Biochem. Sci. *25*, 311–316.
31. Rogers, M.J., Adachi, T., Inokuchi, H., and Söll, D. (1994). Functional communication in the recognition of tRNA by *Escherichia coli* glutaminyl-tRNA synthetase. Proc. Natl. Acad. Sci. USA *91*, 291–295.
32. Weygand-Durasevic, I., Rogers, M.J., and Söll, D. (1994). Connecting anticodon recognition with the active site of *Escherichia coli* glutaminyl-tRNA synthetase. J. Mol. Biol. *240*, 111–118.
33. Sherman, J.M., Thomann, H.-U., and Söll, D. (1996). Functional connectivity between tRNA binding domains in glutaminyl-tRNA synthetase. J. Mol. Biol. *256*, 818–828.
34. Bullock, T.L., Uter, N., Nissan, T.A., and Perona, J.J. (2003). Amino acid discrimination by a class I aminacyl-tRNA synthetase specified by negative determinants. J. Mol. Biol., in press.
35. Perona, J.J., Swanson, R., Rould, M.A., Steitz, T.A., and Söll, D. (1989). Structural basis for misaminoacylation by mutant *E. coli* glutaminyl-tRNA synthetase enzymes. Science *246*, 1152–1154.
36. Inokuchi, H., Hoben, P., Yamao, F., Ozeki, H., and Söll, D. (1984). Transfer RNA mischarging mediated by a mutant Escherichia coli glutaminyl-tRNA synthetase. Proc. Natl. Acad. Sci. USA *81*, 5076–5080.
37. Weygand-Durasevic, I., Schwob, E., and Söll, D. (1993). Acceptor-end binding domain interactions ensure correct aminoacylation of transfer RNA. Proc. Natl. Acad. Sci. USA *90*, 2010–2014.
38. Sherman, J.M., and Söll, D. (1996). Aminoacyl-tRNA synthetases optimize both cognate tRNA recognition and discrimination against noncognate tRNAs. Biochemistry *35*, 601–607.
39. Liu, J., Ibba, M., Hong, K.-W., and Söll, D. (1998). The terminal adenosine of $tRNA^{Gln}$ mediates tRNA-dependent amino acid recognition by glutaminyl-tRNA synthetase. Biochemistry *37*, 9836–9842.
40. Hong, K.-W., Ibba, M., Weygand-Durasevic, I., Rogers, M.J., Thomann, H.-U., and Söll, D. (1996). Transfer RNA-dependent cognate amino acid recognition by an aminoacyl-tRNA synthetase. EMBO J. *15*, 1983–1991.
41. Kern, D., Potier, S., Lapointe, J., and Boulanger, Y. (1980). The glutaminyl-tRNA synthetase of *Escherichia coli*. Purification, structure and function relationship. Biochim. Biophys. Acta *607*, 65–80.
42. Agou, F., Quevillon, S., Kerjan, P., and Mirande, M. (1998). Switching the amino acid specificity of an aminoacyl-tRNA synthetase. Biochemistry *37*, 11309–11314.
43. Williamson, J.R. (2000). Induced fit in RNA-protein recognition. Nat. Struct. Biol. *7*, 834–837.
44. Ribas de Pouplana, L., Auld, D.S., Kim, S., and Schimmel, P. (1996). A mechanism for reducing entropic cost of induced fit in protein-RNA recognition. Biochemistry *35*, 8095–8102.
45. Post, C.B., and Ray, W.J., Jr. (1995). Reexamination of induced fit as a determinant of substrate specificity in enzymatic reactions. Biochemistry *34*, 15881–15885.
46. Hoben, P., Royal, N., Cheung, A., Yamao, F., Biemann, K., and Söll, D. (1982). *Escherichia coli* glutaminyl-tRNA synthetase. J. Biol. Chem. *257*, 11644–11650.
47. Perona, J.J., Swanson, R., Steitz, T.A., and Söll, D. (1988). Overproduction and purification of *Escherichia coli* $tRNA^{Gln}$ and its use in crystallization of the glutaminyl-tRNA synthetase-$tRNA^{Gln}$ complex. J. Mol. Biol. *202*, 121–126.
48. Brünger, A.T., Adams, P.T., Clore, G.M., Delano, W.L., Gros, P., Grosse-Kunstleve, R.W., Jiang, J.S., Kuszewski, J., Nilges, M., Pannu, N.S., et al. (1998). Crystallography and NMR system: a new software suite for macromolecular structure determination. Acta Crystallogr. *D54*, 905–921.
49. Jones, T.A., Zou, J.Y., Cowan, S.W., and Kjeldgaard, M. (1991). Improved methods for building protein models in electron density maps and the location of errors in these models. Acta Crystallogr. *A47*, 110–119.
50. Lu, G. (2000). TOP: a new method for protein structure comparisons and similarity searches. J. Appl. Crystallogr. *33*, 176–183.

Accession Numbers

Coordinates have been submitted to the Protein Data Bank and assigned accession code 1NYL.